Supplementary Information to "Earth system models overestimate the local plant productivity response to temperature–moisture extremes" by M. Adam et al.

In this Supplementary Information (SI), we provide additional figures on the nullmodel's convergence (Sect. S1), significance patterns that overlap between the datasets (Sect. S2), the assignment of IPCC regions to climatic zones (Sect. S3), statistical coupling strength and peak timing (Sect. S4), mechanistic responses (Sect. S5), and mean GPP biases (Sect. S6).

List of Figures

S1 Convergence of the null model

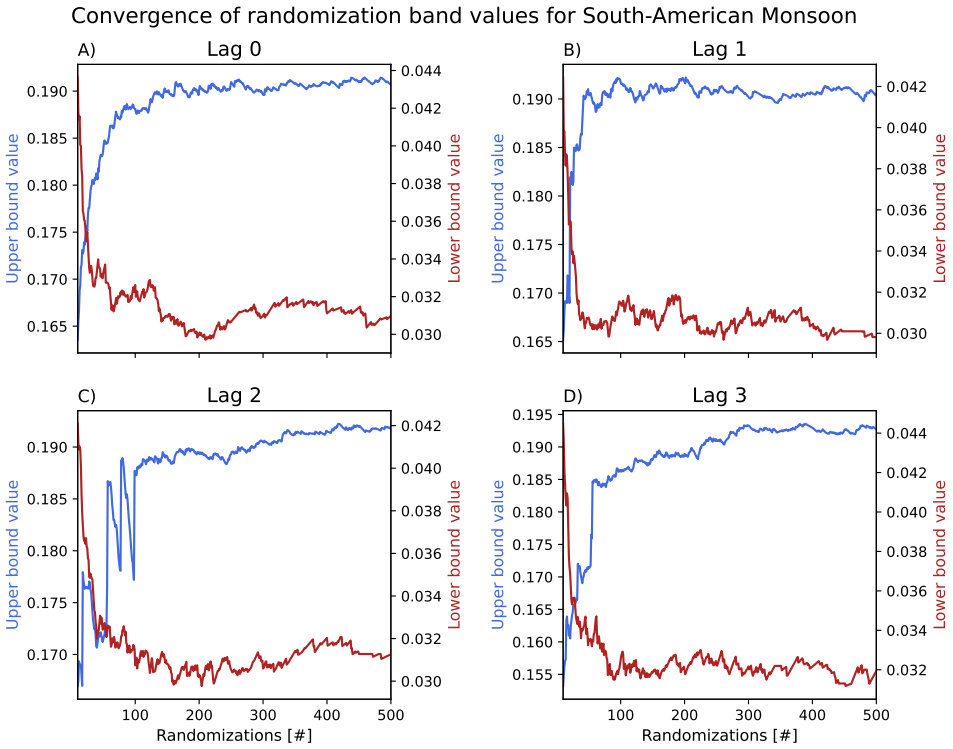

Figure S1 | Nullmodel convergence at different lags between temperature–moisture and GPP extremes. This example covers the South-American Monsoon (see Iturbide et al. (2020)) and reports the 95% range of the nullmodel ensemble as upper and lower bounds in units $^{[COR]}/_{100}$.

S2 Significance patterns and share of significant cells

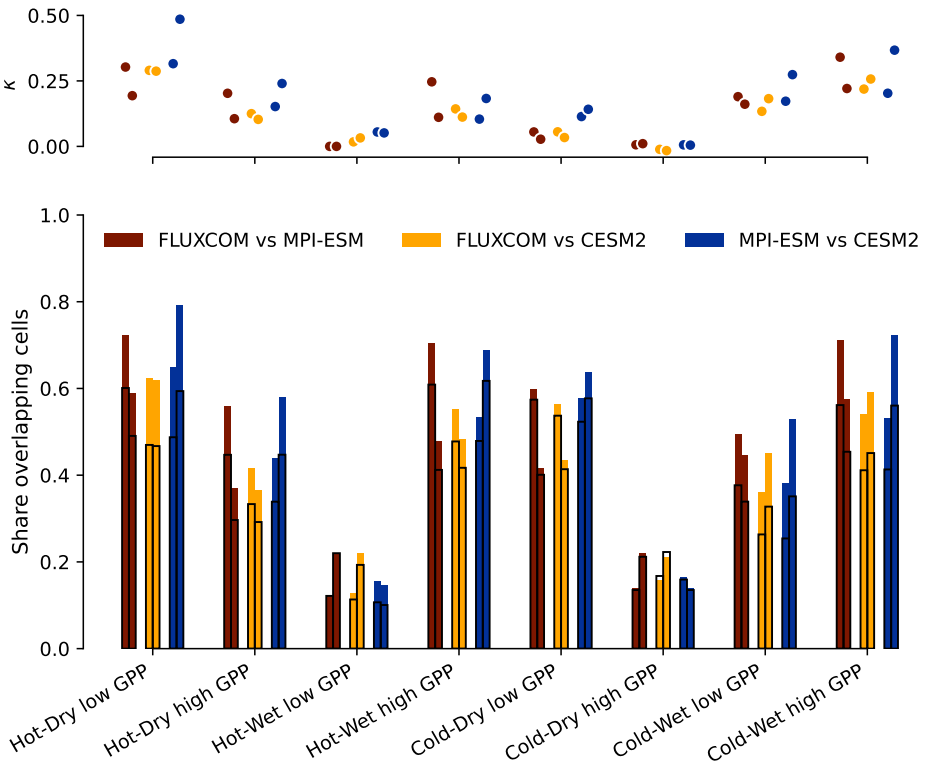

Figure S2 | Overlap between significance patterns in FLUXCOM and the ESMs. Black outlines (bottom panel) represent the average overlap when randomizing the patterns, indicating that patterns overlap by chance. The likelihood of accidentally overlapping patterns is reflected in the κ statistics (upper panel): $\kappa \approx 0$ represents randomness, $\kappa \to 1$ indicates high confidence in the signal.

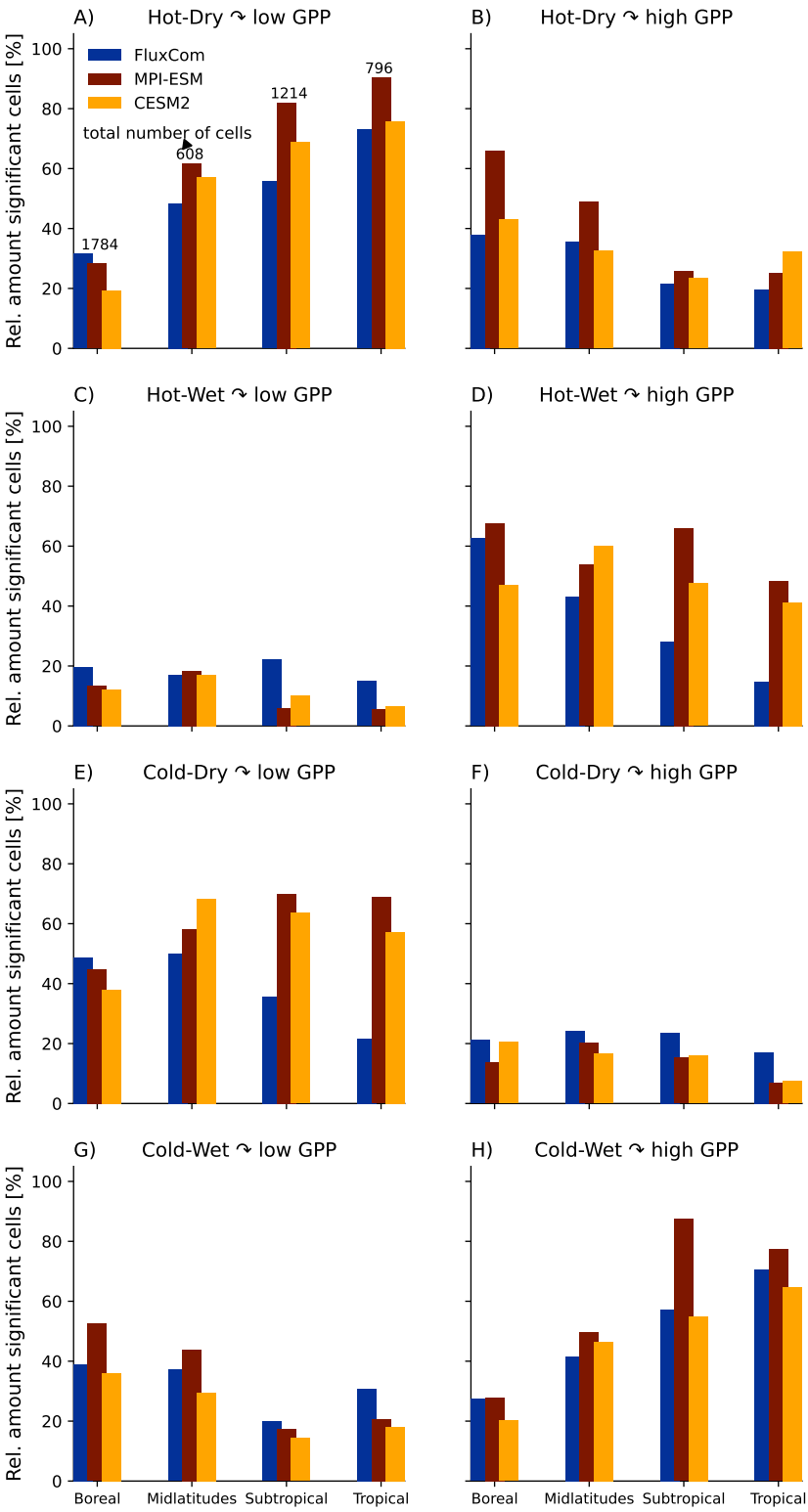

Figure S3 | Share of grid cells with significant statistical coupling between climatic compound and GPP extremes. Here, all grid cells which exceed the null model's 95th quantile at lag one or more are considered significant. Combinations of GPP extremes in the succession of temperature–soil moisture extremes are indicated above individual panels.

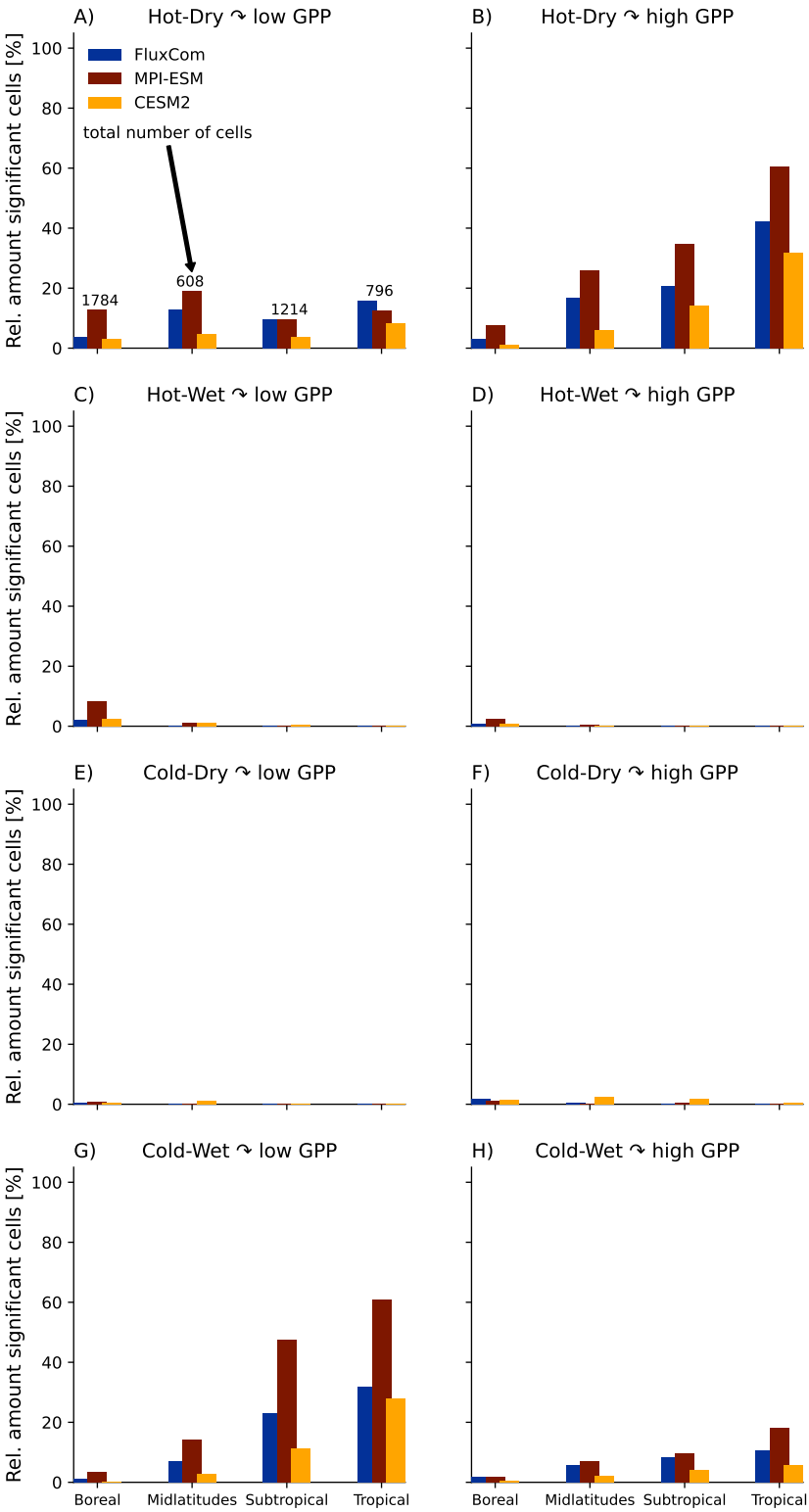

Figure S4 | Analogous to Figure S3 but considering all grid cells which undercut the null model's 5th quantile at lag one or more as significant.

S3 Assignment of IPPC regions to broad climatic zones

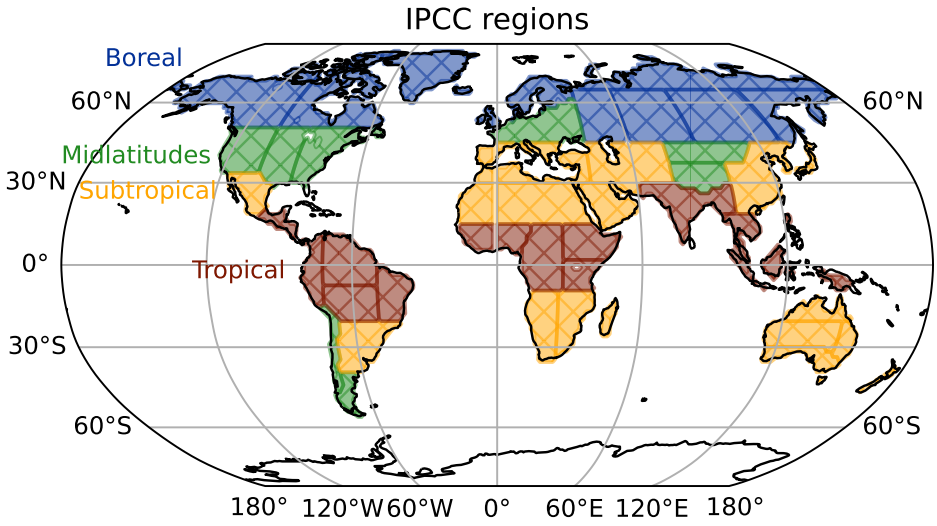

Figure S5 | Assignment of IPPC regions (Iturbide et al., 2020) to broad climatic zones.

S4 Maps of statistical coupling strength and peak timing

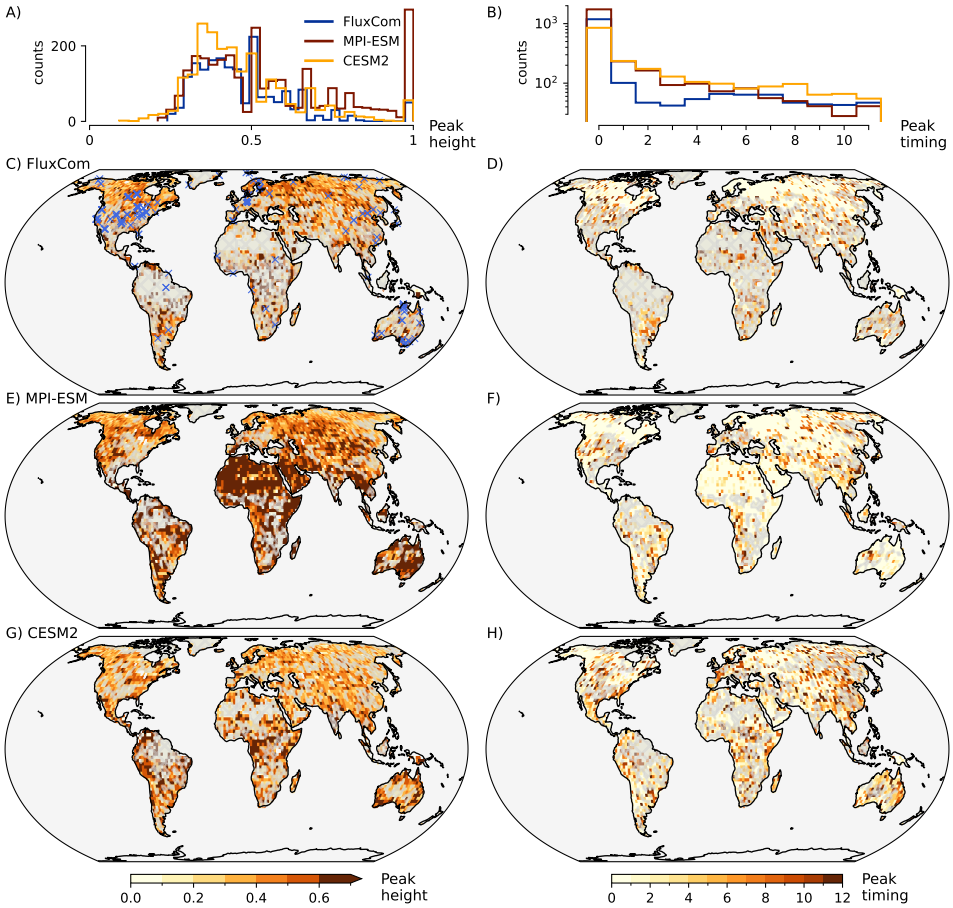

Figure S6 | Highest share of co-occurrences and corresponding timings for hot–wet–high analogous to Fig. 2 of the manuscript.

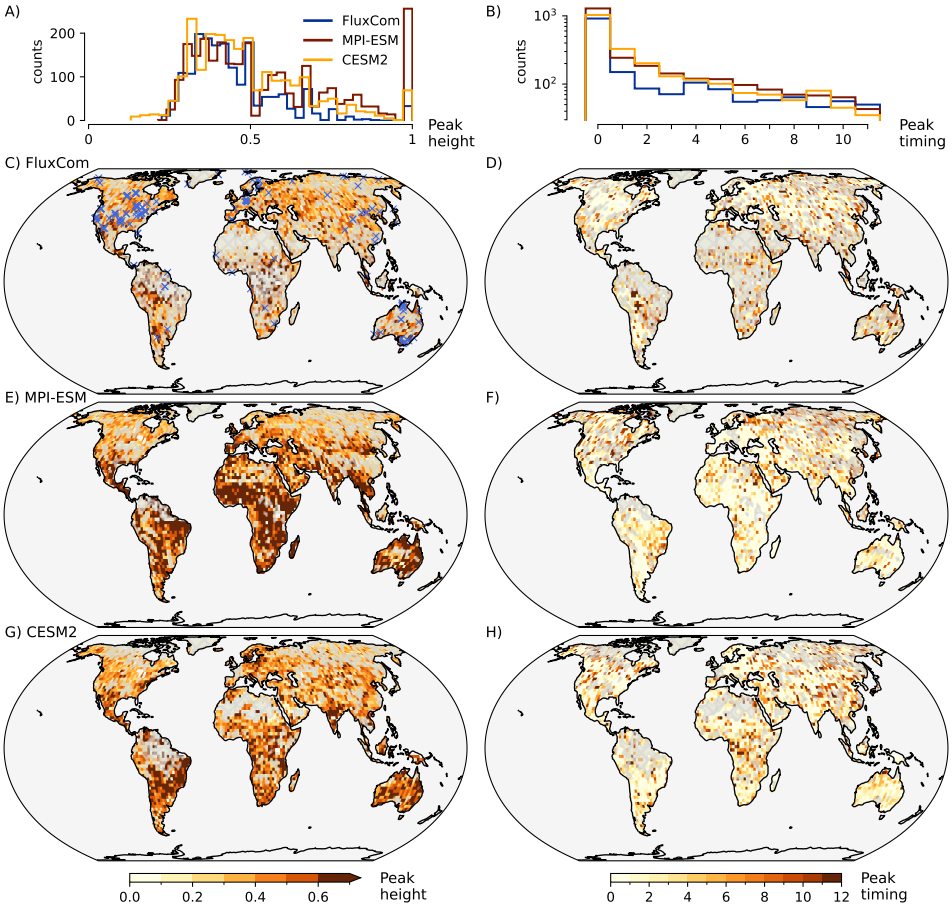

Figure S7 | Analogous to Fig. S6 but for cold–dry–low.

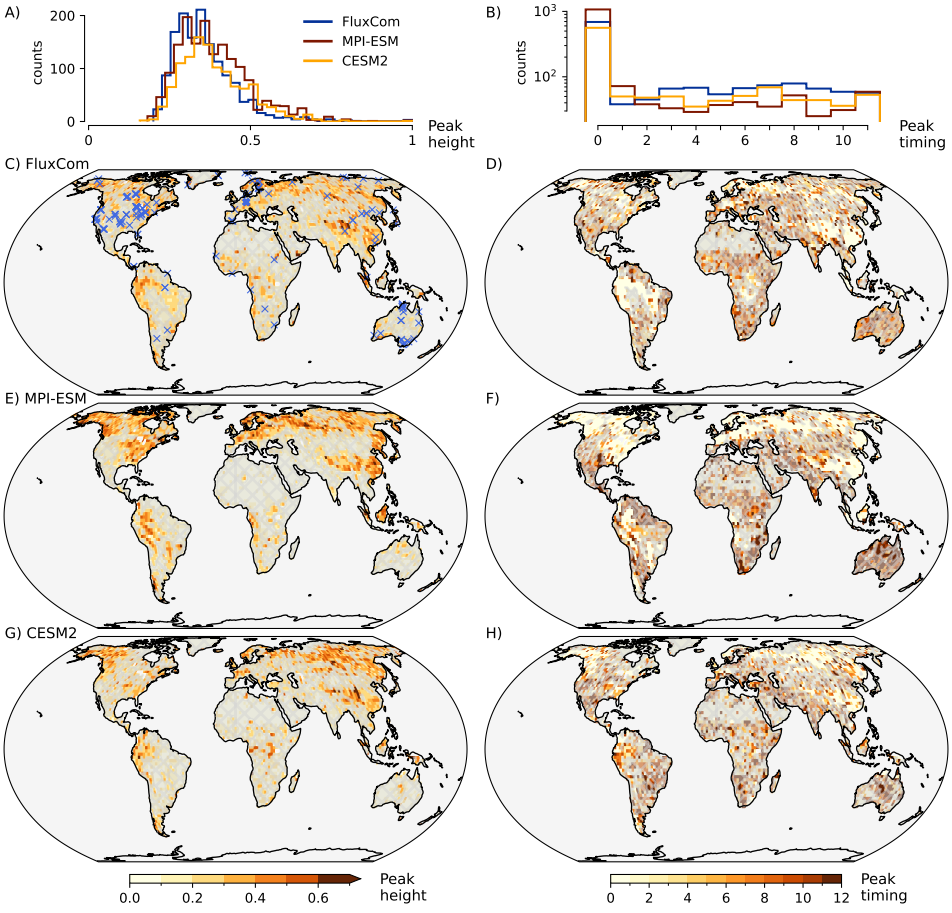

Figure S8 | Analogous to Fig. S6 but for cold–wet–low

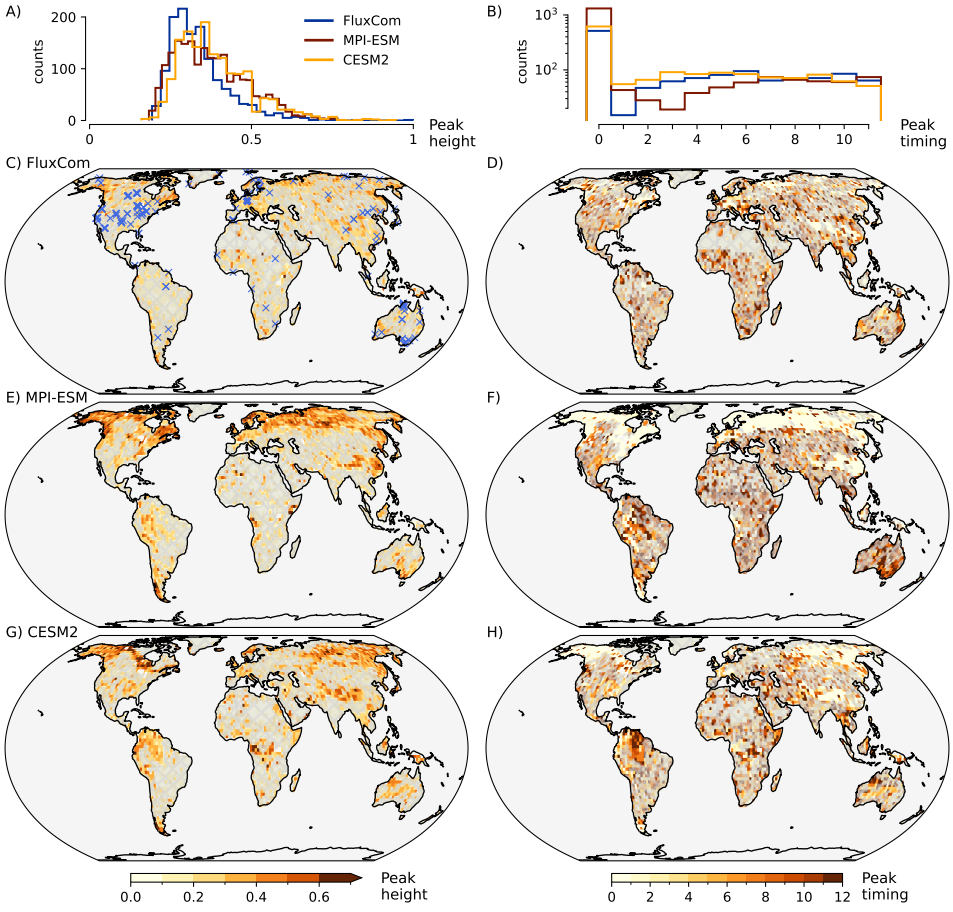

Figure S9 | Analogous to Fig. S6 but for hot–dry–high

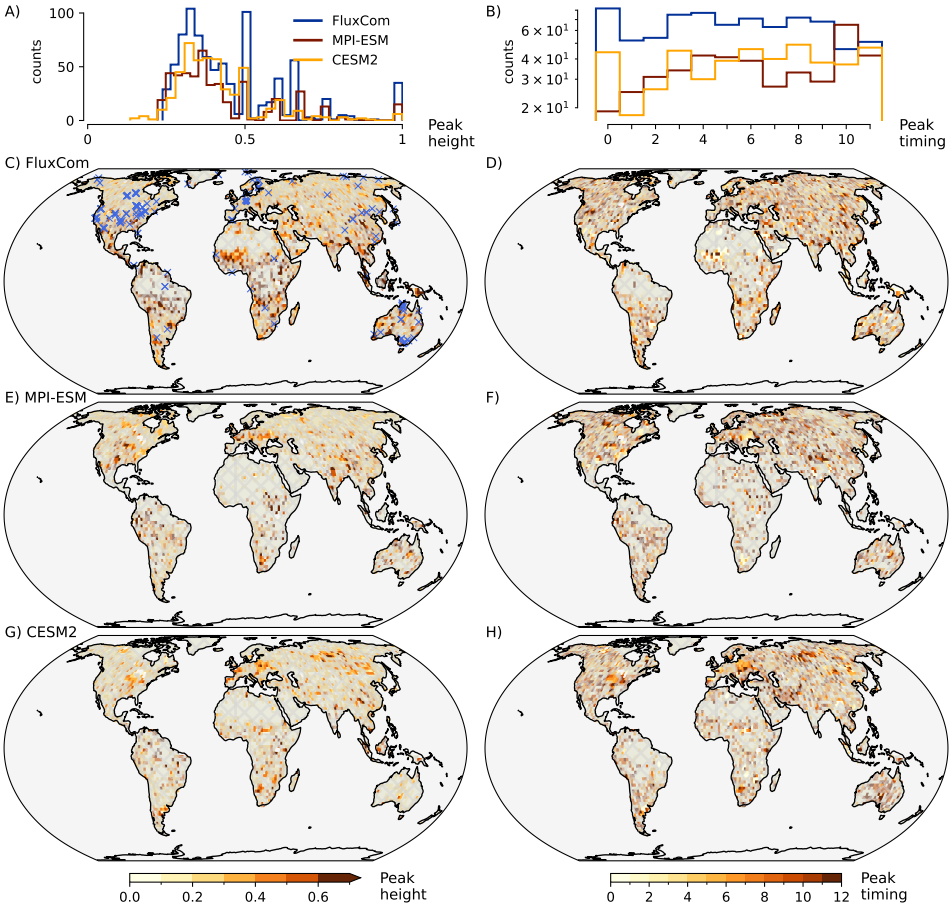

Figure S10 | Analogous to Fig. S6 but for hot–wet–low

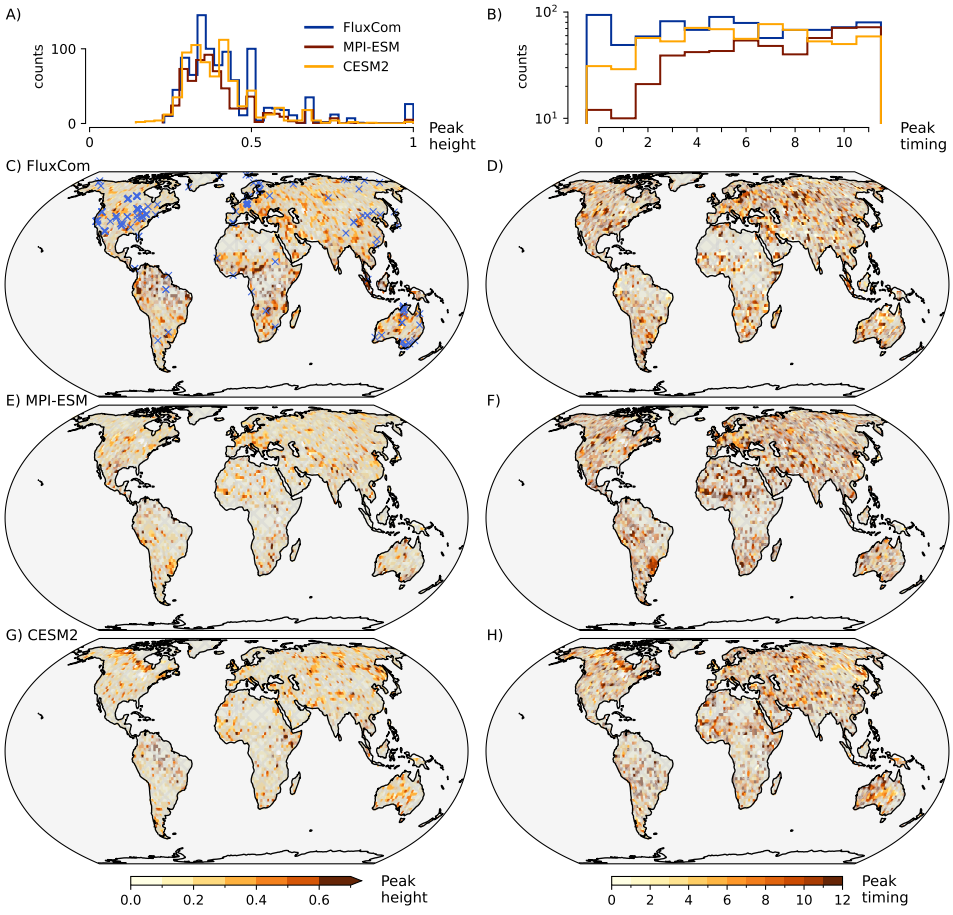

Figure S11 | Analogous to Fig. S6 but for cold–dry–high

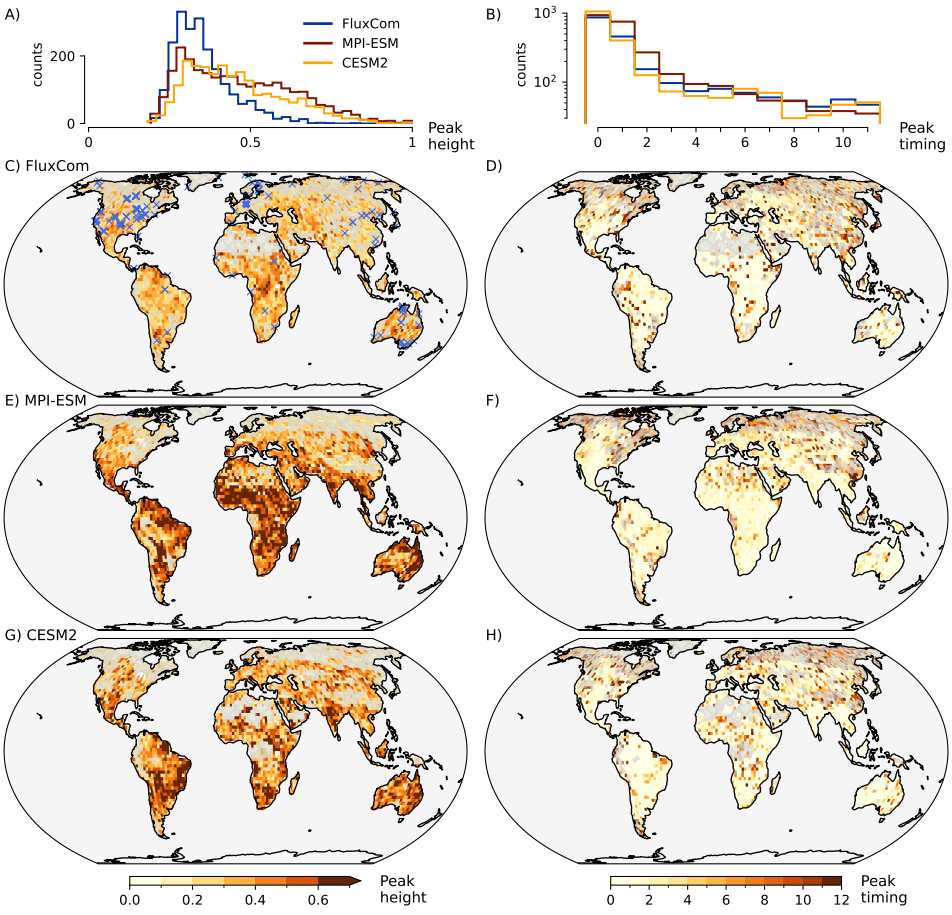

Figure S12 | Analogous to Fig. S6 but for hot–dry–low

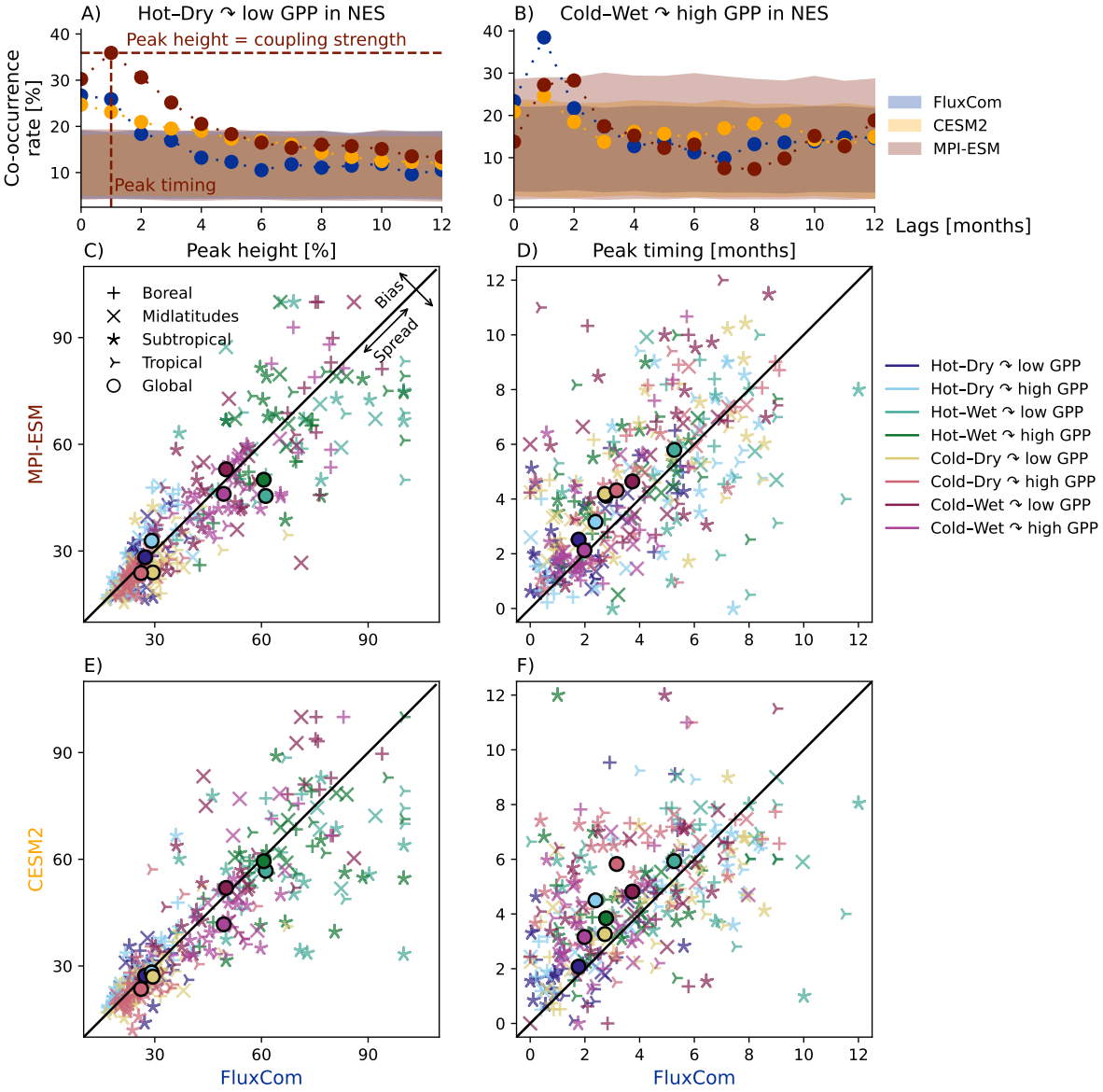

Figure S13 | Agreement in regionally averaged co-occurrence rate and timing between FLUXCOM and the model datasets for precipitation as a moisture indicator. Description analogous to Fig. 4 of the manuscript.

S5 Mechanistic response in the Earth system models

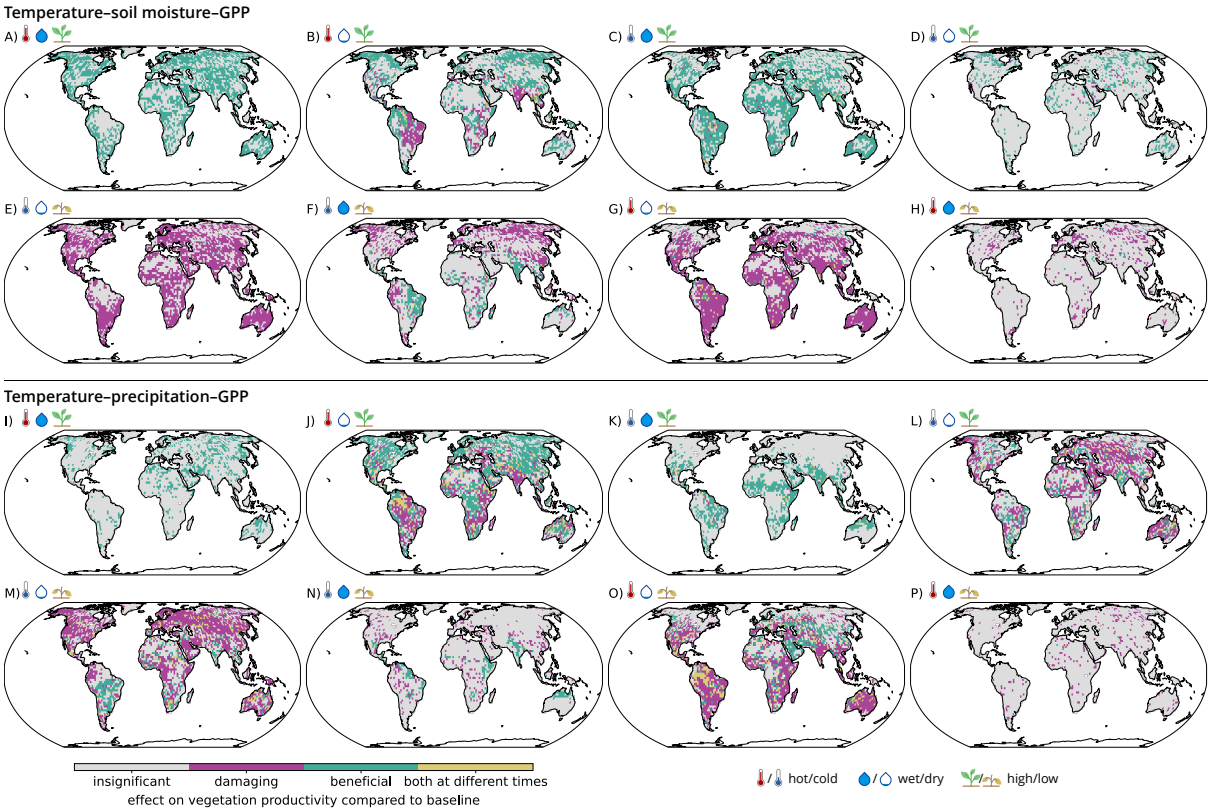

Figure S14 | Categorization of enhanced and muted co-occurrence rates between temperature–soil moisture and GPP extremes and between temperature–precipitation and GPP extremes for CESM2. Description analogous to Fig. 5 of the manuscript.

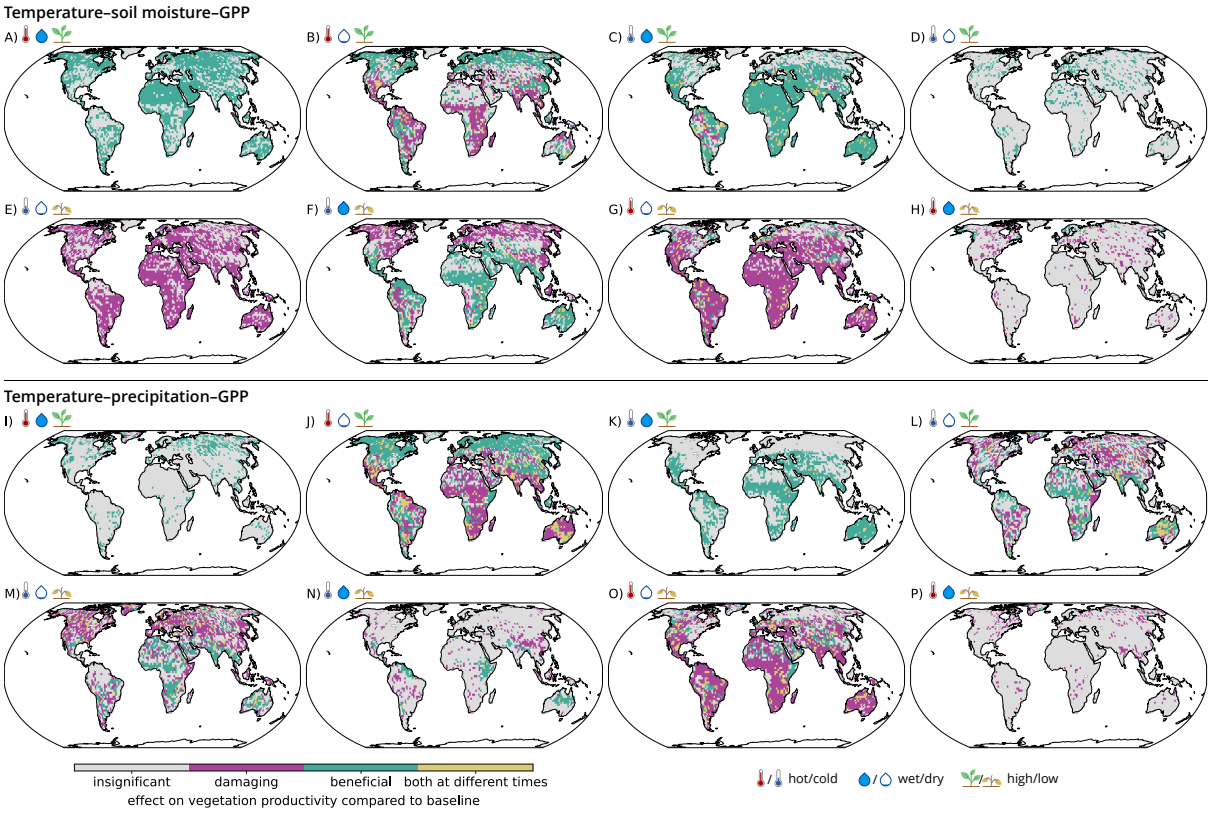

Figure S15 | Analogous to Fig. S14 but for MPI-ESM.

S6 Mean GPP bias in the Earth system models

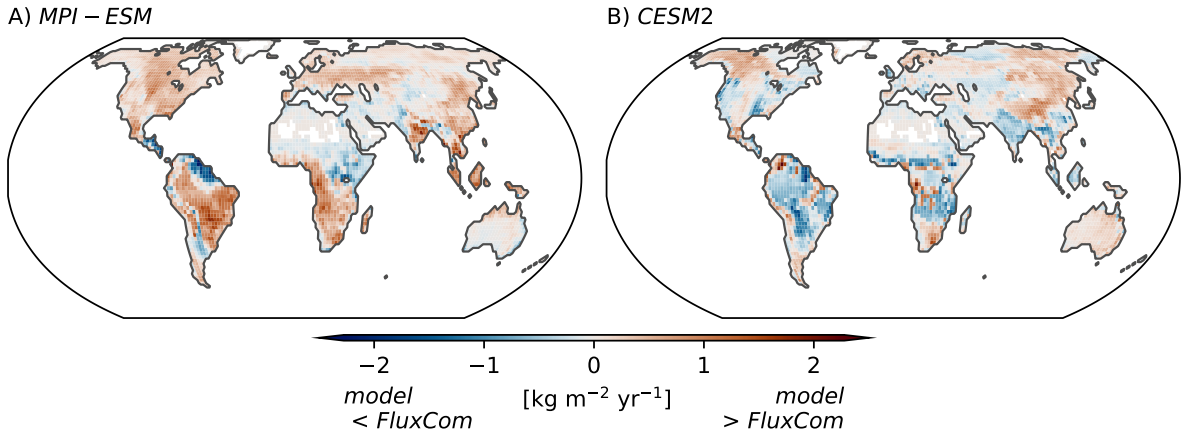

Figure S16 | Mean GPP bias between FLUXCOM and the ESMs. Panels depict the 1999 to 2014 average anomalies to FLUXCOM.